


A Comparative Study Between Oxy-Acetylene and Shielded Metal Arc Welds of AISI 5160 Low Alloy Steel



Abdul Sameea Jasim Jilabi 

Department of Metallurgical Engineering, Faculty of Materials Engineering, University of Babylon, Hillah 51001, Iraq

Corresponding Author Email: sameeakilabi@gmail.com

Copyright: ©2024 The authors. This article is published by IETA and is licensed under the CC BY 4.0 license (<http://creativecommons.org/licenses/by/4.0/>).

<https://doi.org/10.18280/rcma.340404>

ABSTRACT

Received: 28 November 2023

Revised: 29 May 2024

Accepted: 2 July 2024

Available online: 27 August 2024

Keywords:

low alloy steels, oxy-acetylene welding, shielded metal arc welding

Nowadays, low alloy steels effectively contribute to the manufacture of several important products, thus welding these types of steel is of great importance. Two different common welding processes, namely SMAW and OAW using two different fillers (E6013 electrode and A5.2 RG45 wire respectively) were employed to join 6 mm thick AISI 5160 low alloy steel plates. Compared to SMAW, the OAW process resulted in much wider HAZ. Microscopy of both welds revealed that the structure of the weld metal was generally ferrite and pearlite, while that of the unaffected base metal was predominantly pearlite. The structure in the fusion zone and CGHAZ of the oxy-acetylene weld was coarser than that of the SMA weld. Nevertheless, the hardness values across the oxy-acetylene weld were generally lower than those found across the SMA weld. The highest hardness across both welds was in the CGHAZ, while the lowest was in the inter-critical HAZ, and the average hardness in the weld center was lower than that of the base metal. Finally, the average tensile strength value of the SMA weld was much higher than that of the oxy-acetylene weld, where fractography observation revealed porosity and an oxide layer, and the fracture was brittle.

1. INTRODUCTION

Hardenability of steels can generally be controlled by several factors: the chemical composition, the grain size of austenite and the component thickness [1]. Increasing the weight percentage (wt.%) of carbon tends to delay the austenite transformation, providing slower quenching to reduce distortion while retaining hardness. Alloying elements, such as nickel, chromium, manganese and others do not increase the as-quenched hardness of steel as carbon does, but delay the diffusion of carbon within the steel, the diffusion necessary for the formation of pearlite. As a result, the additional alloying elements encourage the formation of martensite at slower cooling rates, and thus enables components to be more hardened [1]. Pearlite nucleation typically occurs at the boundaries of the former austenite grain. Increasing the grain size of austenite decreases the surface area of the grain boundaries for nucleation. The increase of the austenite grain size also delays diffusion of carbon (requires extra travel distance), slowing down the transformation into pearlite and encouraging martensite to form. The coarse-grained heat affected zone (CGHAZ) of steel welds normally owns a large grain size, therefore, martensite may form in this region more easily than predicted. Finally, the component size plays an indirect role in hardenability as it affects cooling rates. During heat treatments, thicker plates may not be easily hardened by quenching due to the variation in heat extraction and thus cooling rates from the surface to the center of the

plates. Thicker steel weld sections, however, result in faster cooling rates that increase the potential for martensite formation. This is because the cooling of thicker plates occurs in three dimensions rather than two [1].

Increasing hardenability is well known to decrease the weldability in steels by increasing the weld's susceptibility to cracking in the weld zone (WZ) and the heat affected zone (HAZ) [2, 3]. The chemical composition of steel, heat input and cooling rate are generally factors result in several effects on welds such as phase changes, grain growth, melting point, expansion and contraction in addition to thermal and electrical conductivity which in turn can determine weldability. Heat input and cooling rate mainly depend on the welding technique used and the thickness of the base metals being welded [4]. Manufacturers aim to achieve as homogeneous properties as possible across the welds. The weld metal properties are largely determined by the filler material selected, the type of the base metal (BM), the welding process used and the welding methodology. The properties of the HAZ are however determined mainly by the BM composition and the amount of heat energy input [5].

During the early part of the nineteenth century, oxy-acetylene welding (OAW) became the main welding process, both for fabrication and construction and for maintenance and repair. It had wide applications as it can be used to weld almost all major metals [6]. It is a versatile process, using simple, easily portable and relatively inexpensive equipment. Its equipment is also self-contained, widely available and easy to

learn. In addition, metals up to about 6 mm thick can be welded by a square butt joint [7, 8]. With the OAW process, heat is created by the combustion of acetylene gas in oxygen giving a high-temperature flame, reaching around 3100°C. This flame temperature is generally lower compared to the electric arc temperature, resulting in lower thermal concentration. The flame is then directed towards the joint to be melted, and filler material can be introduced to fill the gap if needed. A less concentrated heat flame results in a better temperature balance in the weld, and therefore slower cooling. Slow heating and cooling rates have an advantage when welding hardenable steels by avoiding the risk of weld cracks. This however makes the process relatively slow with higher heat inputs, increasing the HAZ width of the welds and the risks of thermal stresses and distortion [5]. In addition to the safety issues that must be considered with the process, another drawback is that the oxy-acetylene weld appearance is much rougher than that of the other welding processes, and more finishing might be required [7, 9]. Today, many of the major metals such as aluminum, titanium and stainless steel can be welded more easily using other processes. The oxy-acetylene process is still used to perform operations such as soldering, brazing and welding low melting metals as well as general maintenance and repair work. Gas welding is often preferred for pipes and tubes being welded in very confined spaces [7, 8]. Although the OAW is not used as before, it still has wide applications that make it a necessary process [6]. It is efficient and economical for applications such as welding of small diameter pipes, construction and repairing of heating, ventilation and air conditioning systems. Other applications of OAW include welding of gas cylinders, hot water pipes, boilers and nuclear heat exchangers [8].

Furthermore, shielded metal arc welding (SMAW) remains universally the most extensively used process. In some countries, it accounts for more than half of all welding techniques employed. Coalescence of metals is achieved through heat generated by an electric arc formed between the tip of a covered consumable electrode and the surface of the joint to be welded. The arc is moved along the joint with appropriate length and travel speed, melting the covered electrode with a portion of the BM while the arc progresses. Therefore, the electrode core has two functions are conducting an electric current to the arc, and providing a filler metal for the joint. The main objectives of the electrode covering are providing shielding gases to protect the molten metal from atmosphere contamination and improving the stability of the arc. The shielding used, along with other ingredients of the electrode covering and the electrode core wire, greatly control the chemical composition, mechanical properties and

microstructure of the weld metal, as well as the characteristics of the arc [10]. Due to its affordability, simplicity and versatility, the SMAW technique is nowadays the premier in repair and maintenance work, and is largely employed in the construction of steel structures. Its wide range of applications and cost-efficient equipment make it the preferred choice for small factories and workshops, where automation is often unnecessary and/or uneconomical. Additionally, SMAW provides inherent gas protection, making it less susceptible to wind draft compared to processes that use inert gases for protection [11].

The effects of different welding variables such as heat input, cooling rates, post-weld heat treatment, type of filler material, current values and travel speeds on carbon steels welded using various fusion welding processes have been broadly studied. The researches [12-15] dealt with studying the effects of welding variables on shielded metal arc (SMA) welds of low carbon steels. Few articles [16, 17], however, have been found that compare between oxy-acetylene and SMA welds, but of low carbon steels. Bodude and Momohjimoh [16] revealed in 2015 that the tensile strength and hardness decrease with increasing heat input into both oxy-acetylene and SMA welds. Cooling rates also showed a significant impact on the structure of the welds, where the presence of pearlite and ferrite was observed in different proportions under various conditions. On the other hand, Fathi et al. [17] suggested that the tensile strength produced using oxy-acetylene welding of mild steel was higher compared to that achieved using the SMAW process, but the hardness was lower.

As of writing this paper, the researcher had not found such investigative and comparative studies for welds made of low alloy steels. The aim of the present study is investigating and comparing the mechanical properties (tensile and hardness), microstructure and HAZ width caused by OAW and SMAW of AISI 5160 low alloy steel. AISI 5160 has high ductility, high tensile strength and excellent toughness that qualify it for several important industrial applications in machinery and heavy equipment [18], which could require welding, where replacing the entire component might be impractical.

2. EXPERIMENTAL DETAILS

2.1 Base material

Table 1 displays the alloy used in the present work as a BM based on AISI standards [18], while Table 2 confirms that the actual composition of the raw material is within these AISI compositional ranges.

Table 1. Standards of the alloy used in this study as a BM along with its elemental composition

Alloy	Elemental Composition (wt.%)						Std. Symbol (AISI)	Form and C.S. of Raw Material (mm)	Ultimate Tensile Strength (MPa)	Vickers Hardness (HV)	Raw material Condition
	C	Mn	Si	Cr	P max.	S max.					
Low alloy steel	0.56-0.64	0.75-1.0	0.15-0.3	0.7-0.9	0.035	0.04	5160	Plate (7×70)	724	207	Annealed and cold drawn

Table 2. Actual elemental composition of the AISI 5160 low alloy steel employed as a BM

Base metal	Elemental Composition (wt.%)					
	C	Mn	Si	Cr	Mo	P, S
Low alloy steel	0.6	0.86	0.17	0.8	0.03	0.04

2.2 Electrode used with the SMAW process

Specifications of the welding electrode employed as a filler material in the SMAW process are detailed in Table 3 based on the American Welding Society (AWS) [19].

Table 3. Electrode specifications based on the AWS [19]

Electrode with Dia. of Ø 3.2 mm	Electrode Sort	Coating Class	Wire Metal Type	Typical Properties All Weld Metal			Typical All Weld Metal Composition (wt.%)			
				T.S.(MPa)	Y.S.(MPa)	EL.(%)	C	Mn	Si	Fe
E6013	Rutile	Titania-Potassium	Mild steel	510	400	28	0.08	0.4	0.3	Balanced

Table 4. Steel rod specifications according to AWS [20]

Copper Coated Mild Steel Rod	Rod Metal Type	T.S. (MPa)	Covering Gas	Wire chemical composition % (max.)									
				C	Mn	Si	Cr	Ni	Cu	Mo	Al	P	S
AWS A5.2 RG45 solid wire	Low carbon steel	310	None	0.08	0.05	0.1	0.2	0.3	.3	0.2	0.02	0.035	0.04

2.4 Welding of AISI 5160 low alloy steel

The operations below were carefully carried out before the welding process began. A square butt weld joint is illustrated in Figure 1, along with the dimensions of the plates to be welded on both sides.

(1) Remove rust up to half a millimeter from both surfaces of the plates being welded before cleaning from grease, oils and other impurities.

(2) Furnace-dehydrating the E6013 welding electrodes, involving a gradual temperature increase to 135°C in accordance with AWS recommendations.

(3) Fitting-up the plates being welded with a 2.5mm gap (Figure 1), before tack welding, and remove the slag formed.

(4) Adjust the welding current value of the E6013 electrode according to AWS and the manufacturer's recommendations for these electrodes.

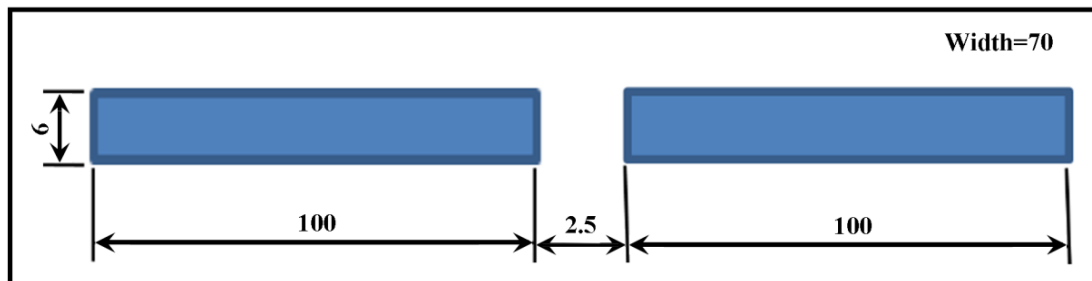


Figure 1. Weld joint employed in this study (DIMS in mm)

Table 5. Welding parameters of the AISI 5160 steel plates

Welding by the Utilize of Welding Parameters	E6013 Electrode (SMAW)	RG45 Solid Wire (OAW)
Current value (A)	100	-
Electrode/Rod dia. (mm)	3.2	3.175
Current/Flame class	DCEP	Oxidizing
Position	Flat	

SMAW and OAW for the 6 mm thick AISI 5160 steel tack-welded plates were then achieved using the E6013 electrode and RG45 solid wire respectively. Welding was initially applied on one side of the joint. The formed slag was then carefully removed prior to welding the opposite side. Table 5 shows the welding parameters utilized in this work for both SMAW and OAW techniques, knowing that the welding was performed under the workshop atmosphere.

2.5 Microscopy

Specimens for optical microscopy were prepared following established metallographic practices (according to ASTM E 407-2015 and ASTM E3-2017). After cold saw cutting, the specimen surface was subjected to wet grinding using a

motorized rotary disc equipped with silicon carbide abrasive papers of multiple grit sizes (180, 220, 320, 400, 600, 800, 1000, 1200 and 1500) in a sequential order.

Mechanical polishing with a series of diamond pastes of grit sizes ranging from 3 to 0.25 µm was then employed to remove any residual scratches introduced during grinding. The final step of specimen preparation involved etching the polished surface with a 2% nital solution. This is to enhance contrast between various constituents within the microstructure. The function of specimen preparation is to identify the microstructures as well as the topography of different regions across the welds under study including the WZ and HAZ. Examination of these specimens also aimed to determine, categorize and analyze any potential faults present on the weld surfaces.

2.6 Microhardness test

Vickers microhardness test was performed across the welds on the ground and polished surfaces under a load of 500 g for 10 s by 1 mm intervals at a rate of three tests for each point.

2.7 Tensile examination

The weld tensile strength value was an average of three specimens prepared based on ASTM [21] shown in Figure 2. The weld was placed at the centre of the specimen.

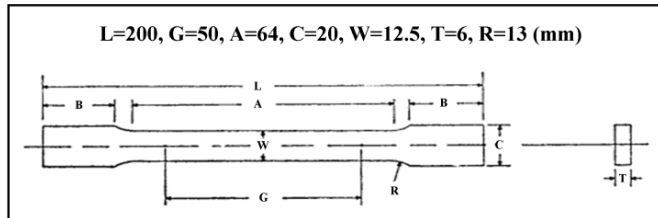


Figure 2. The specimen of the tensile test based on ASTM

2.8 Fractography observation

This visual inspection was achieved by photographing the fracture surface of the tensile specimens to determine the type, size and location of internal defects (including cracks and slag inclusions) that could be easily observed with the naked eye.

3. RESULTS AND DISCUSSION

The square butt was chosen as a weld joint for being the most common design, and is appropriate to the thickness of the pieces being welded in this study. Besides, this design does not require edge preparation except for traditional cleaning [2].

Figure 3 shows that the visual extension of the HAZ from the weld center on both sides of the oxy-acetylene weld was 7.96cm, while in the SMA weld it was 2.36cm. This is due to the fact that the temperatures generated by the gas welding processes are, in general, much lower than those of the electric arc welding processes. So, to achieve a successful oxy-acetylene weld, prolonged heating is necessary. The amount of heat input, and thus the HAZ width will therefore be more. Other disadvantages of the prolonged heating are grain growth, distortion and lack of corrosion resistance in some cases [22].



Figure 3. Visual HAZ extension of (1): Oxy-acetylene weld and (2): SMA weld

Microstructural analysis of the AISI 5160 steel welds joined with the OAW and SMAW processes exhibited two particular zones in each weld, called the WZ and HAZ. Based on the filler material employed, the weld metal microstructure changed. This analysis also revealed changes in the HAZ beginning from the region adjacent to the WZ reaching to the BM unaffected by heat. These microstructural changes are attributed to the relatively steep thermal slope that the HAZ suffers from melting temperature (T_m) to the unaffected BM temperature. Following, a rapid cooling rate will occur due to the comparatively cold adjoining BM and the aerosphere. This thermal cycle is actually various heat treatments for HAZ regions. As is known, the variance in the microstructures leads to a difference in characteristics and thus in performance [23].

Figure 4(a) shows that the BM microstructure consists mostly of pearlite lamellae with a slight quantity of intergranular ferrite based on the elemental composition and condition of the base material shown in Table 1. Figure 4(b) illustrates the microstructure of the WZ of the AISI 5160 steel weld joined by the SMAW process. It consists of equiaxed crystals of ferrite and pearlite. While examining the microstructure of this weld, no cracking was detected in the WZ.

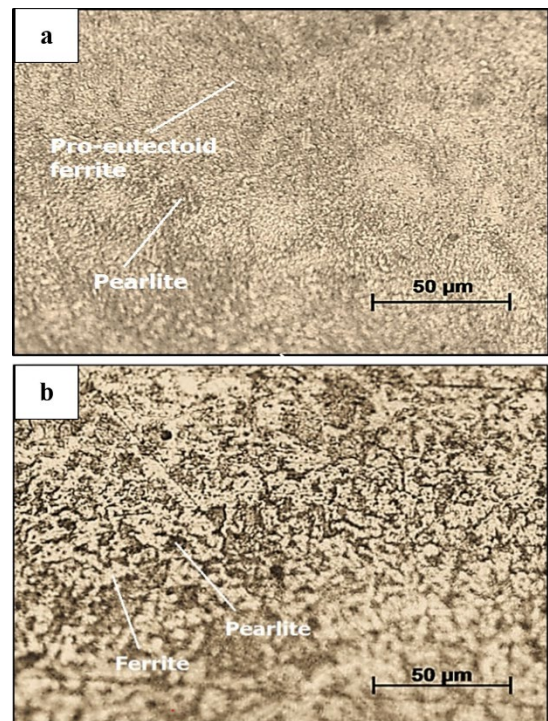


Figure 4. Optical microstructure of the (a): AISI 5160 steel BM; (b): Shielded metal arc WZ

The CGHAZ structure, immediately adjoining to the WZ, mostly contained colonies of pearlite larger than those in the BM with a minor quantity of ferrite Figure 5(a). This region experiences the highest temperatures among the HAZ regions, so grain growth occurs. The particle size of pearlite relies on the austenite granular size. Progressing from the centerline of the weld joint, the particle size of pearlite gradually decreases until the fine-grained region (FGHAZ) that experiences lower temperatures so that a slight growth occurs and thus the particles remain finer. The microstructure of this region exhibits a particle size of pearlite smaller than that of the BM Figure 5(b).

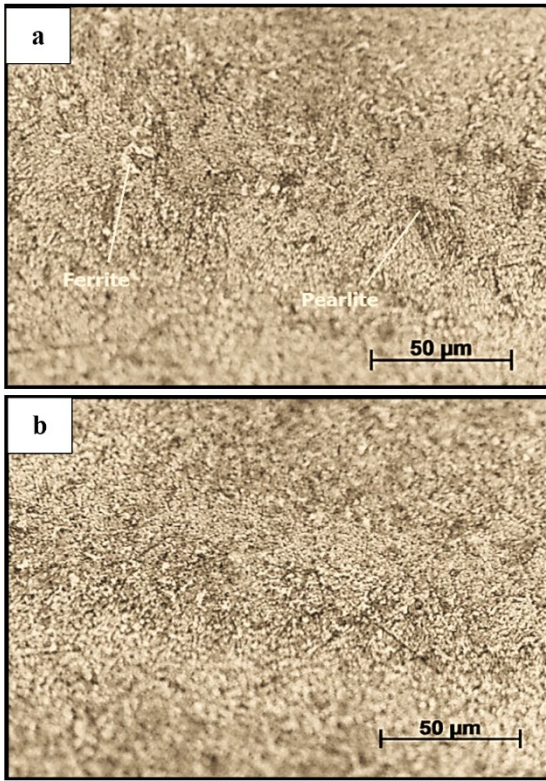


Figure 5. Optical microstructure of the (a): CGHAZ; (b): FGHAZ of the SMA weld

Figure 6(a) illustrates the microstructure of the inter-critical HAZ (transition zone), closely adjoining to the FGHAZ. The microstructure with the smallest particle size across the weld could be noted in this zone, as the pearlite was partially spheroidized. This is consistent with that revealed in 2021 by Jilabi [24] shown in Figure 6(b).

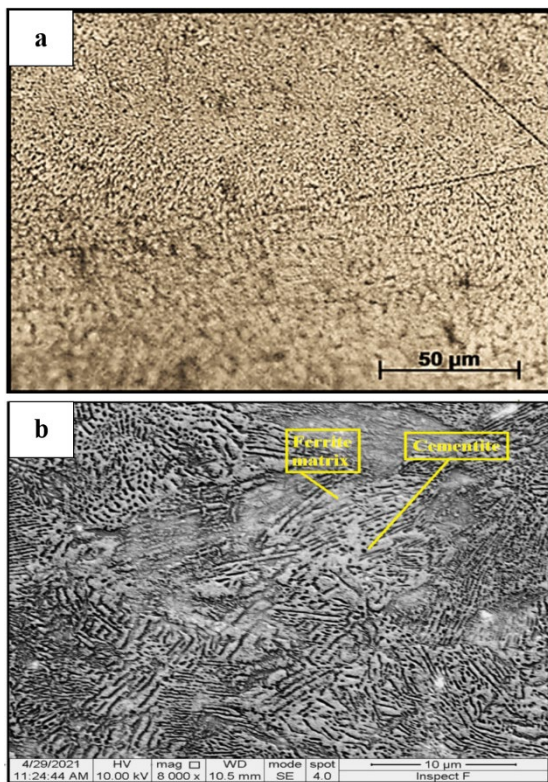


Figure 6. (a): Optical structure of the inter-critical HAZ of the SMA weld; (b): SEM micrography [24]

Microscopy also revealed that the WZ structure of the AISI 5160 steel weld joined by the OAW process consists of intergranular ferrite along with pearlite lamellae in addition to dendritic growth of ferrite within the pearlite colonies Figure 7(a). The microstructure of the CGHAZ of this weld was a proeutectoid ferrite along former austenite grain boundaries with coarse pearlitic colonies and a small amount of ferrite Figure 7(b). Other regions of the HAZ were similar to those of the SMA weld Figure 7(c)-(d).

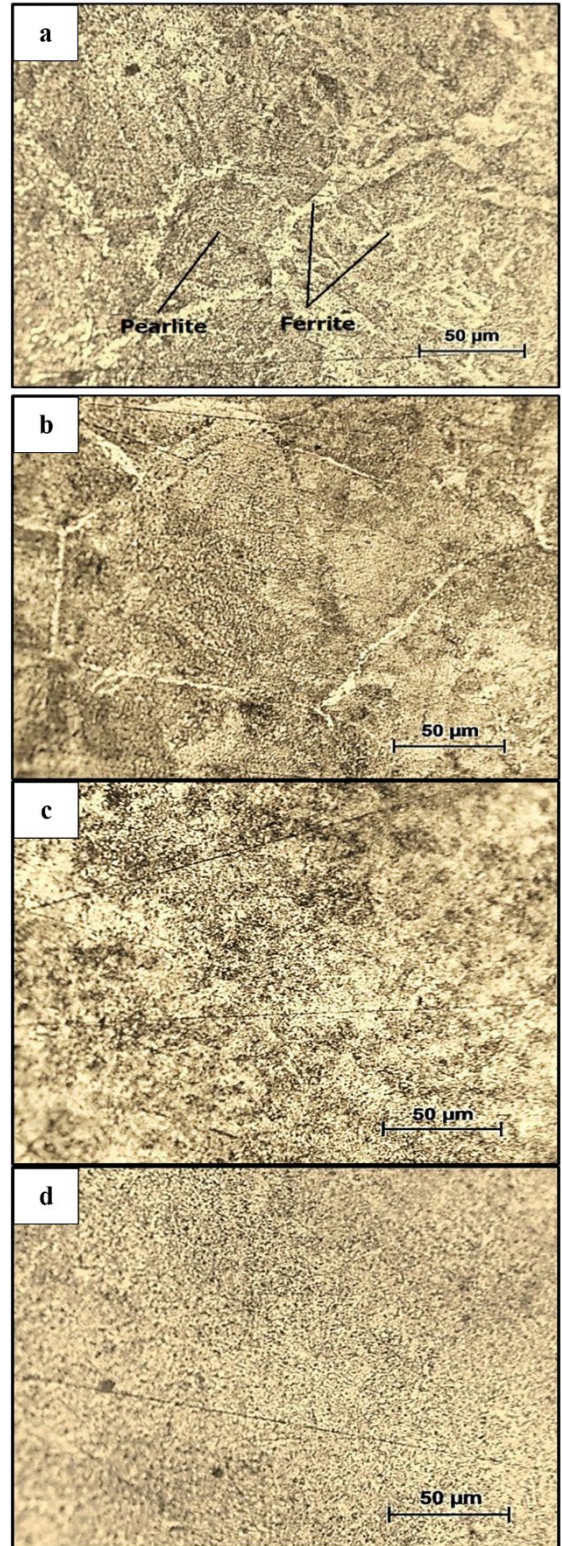


Figure 7. Optical microstructure of the (a): WZ; (b): CGHAZ; (c): FGHAZ; (d): Inter-critical HAZ of the oxy-acetylene AISI 5160 low alloy steel weld

It is clearly observed from the microstructures of both SMA and oxy-acetylene welds that the structure of the WZ was generally ferrite and pearlite. The reason behind this is that the deposited weld metal consists mainly of a filler material which is mostly of low carbon steel (Tables 3 and 4), in addition to a part of the molten BM; a pearlitic microstructure Figure 4(a). Microscopic observation revealed that the pearlite structure in the CGHAZ region of the oxy-acetylene weld Figure 7(b) was much coarser than that of the SMA weld Figure 5(a). This can be attributed to the prolonged heating associated with the OAW process and thus more grain growth resulting in a coarser pearlite. The WZ of the oxy-acetylene weld was coarser as well due to the slow cooling rate associated. This is in consistent with the findings of Odebiyi et al. [25] in 2019.

Since the FGHAZ region undergoes a heat cycle analogous to normalizing treatment commonly used for carbon steels, its properties are likely comparable to those of normalized steel. Due to the prolonged heating used in the OAW process, the spheroidizing the cementite within the pearlite is expected to be more in the oxy-acetylene weld.

Due to the variances in microstructure through the welds, the hardness distribution is expected to vary too. Figure 8(a) shows the variation in hardness across the AISI 5160 steel weld joined by the SMAW process. While slightly proceeding from the center of the weld (p.1), the average hardness steeply rises from (123HV) to reach a peak of (380HV) at almost 2 mm away from the center (p.2). The hardness then drops to a value of (182HV) at approximately 8 mm from the center (p.3), before increasing to that of the BM (234HV) at 16 mm away from the weld center (p.4).

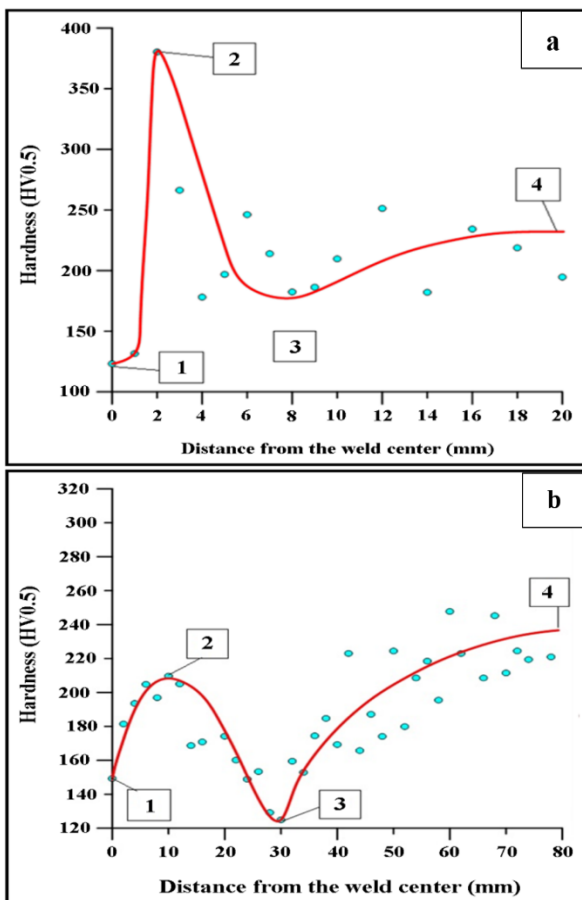


Figure 8. Hardness variations across: (a): SMA; (b): oxy-acetylene welds; (1) the weld center; (2): CGHAZ; (3): ICHAZ; (4): unaffected BM

On the other hand, Figure 8(b) shows the hardness variation across the oxy-acetylene weld. The average hardness value increases on advancing from the weld center (149HV) reaching a value of (210HV) at 10mm away from the center (p.2). The rise in hardness value was not as steep as that caused by the SMAW process. Thereafter, the hardness drops to a minimum of (125HV) at nearly 30mm away from the center (p.3), before increasing to that of the BM (235HV) at approximately 80mm from the center (p.4).

The average hardness at the center of both welds is lower compared to the BM hardness. The cause for this is the higher percentage of soft ferrite phase in the microstructures of the WZ (Figures 4(a), 4(b) and 7(a)). This is because the deposited weld metal is mainly composed of the filler metal and a part of the BM. The filler metals used with both welds were generally made of low carbon steels (Tables 3 and 4). Figures 4(b) and 7(a) however show that the ferrite percentage in the SMA weld is greater compared to that in the oxy-acetylene weld.

The highest hardness across both welds was a slight distance from the center of the weld. A potential reason for this increased hardness is the lack of the soft (easily deformed) ferrite phase in the structure of this region (Figures 5(a) and 7(b)). Moreover, the CGHAZ, as a result of the steeper thermal gradient, experiences a faster cooling rate compared to other HAZs. Since faster cooling rates cause finer interlamellar spacings of pearlite [26], the hardness in this region is therefore enhanced. The intercritical HAZ, characterized by a partially spheroidized pearlitic structure Figures 6 and 7(d), exhibits the lowest hardness across the welds. This can be attributed to the fact that this structure consists of dispersed, partially spheroidized cementite within a matrix of soft ferrite, resulting in an overall lower hardness in this region. The average hardness value of this region in the oxy-acetylene weld was lower compared to that in the SMA weld. This might be due to the prolonged heating used with the OAW process, which can provide a sufficient time for further spheroidizing the cementite to produce a soft, low hardness ferrite matrix. In general, prolonged heating made the hardness of the oxy-acetylene weld lower than that of the SMA weld due to more heat input being provided, resulting in slower cooling rates [26]. This is in agreement with the results of the [16] and [17].

For this study, AISI 5160 steel was selected as a BM due to its reputation as a low alloy steel that is difficult to weld. This challenge is attributed to its high hardenability, caused by relatively high carbon and alloying element contents [3, 23]. The fracture location in all tensile test specimens within the WZ confirms that the obtained results accurately reflect the tensile strength of the weld metal. Meanwhile, the joint efficiency for each weld can be evaluated employing the following equation [23], where the BM's ultimate tensile strength is 724MPa, as presented in Table 1.

$$\text{Weld joint efficiency (\%)} = \frac{\text{Weld metal tensile strength}}{\text{Base metal tensile strength}} * 100$$

The findings revealed that the tensile strength and joint efficiency of the oxy-acetylene weld (34.6MPa and 4.8% respectively) are very low. This may be due to the lack of smelting (poor fusion) as a result of using BM of a relatively large thickness (6 mm), while the appropriate thickness for the BM being welded by the OAW process is preferred to be (1-2 mm) [23]. Moreover, flux was not used during this process whose the main function is to generate covering gases that isolate the molten or hot WZ (fracture region) from

atmospheric pollutants such as oxygen, nitrogen, hydrogen, carbon dioxide and water vapour. These pollutants contribute to the formation of porosity and oxidation of the metal. Oxides however are known as brittle non-metallic materials that increase the brittleness of metals [23]. Both porosity and oxide layers revealed by fractography observation in Figure 9(a), made the tensile strength of the oxy-acetylene weld deteriorates. In 2015, Bodude and Momohjimoh [16] found that the tensile strength decreases with increasing heat input into the weld as in the case with the OAW process. This contradicts what was suggested in 2019 by Fathi et al. [17].

For the tensile test specimens of the SMA weld, although the fracture occurred in the WZ, the average tensile strength value was 534MPa, which is equivalent to 73.8% of the BM tensile strength. This tensile strength satisfies the requirements for a variety of engineering applications, and its relatively high value could be due to the completion of fusion, and to the use of welding electrodes coated with the flux (E6013). The tensile strength and thus weld joint efficiency could have been greater than those reached in this study, as the (E6013) electrode is specially made for welding mild steel, not low alloy steels [19]. This is because it is a cellulose (high hydrogen covering) electrode, exposing the hardenable steel welds to cracking, and thus reducing the tensile strength of the welds, as well as causing porosity being a highly hydrogen covering electrode [2, 27]. Additionally, the presence of slag inclusions in the WZ, as fractography observation revealed in one of the weld specimens Figure 9(b), could be a contributing factor to the reduction in tensile strength of the SMA weld. The appearance of few slag inclusions can be attributed to the fact that the deposition rate of the SMAW process is greater than that of the OAW process. This translates to faster weld travel speeds, which in turn result in quicker cooling rates due to reduced heat input. Rapid cooling can restrict the time available for slag to float to the surface of the weld pool, potentially increasing the risk of trapped inclusions. The almost ductile fracture appeared in the other specimen of the SMA weld Figure 9(c) might be attributed to the type of welding electrode (E6013) used, which is made of mild steel (Table 3). This electrode was used in this paper, being the least expensive and most common. The electrode covering contains a relatively high ratio of materials that ionized easily while heated by the electric arc, such as titania and potassium, thus increases the arc stability during welding and facilitates ignition [19].

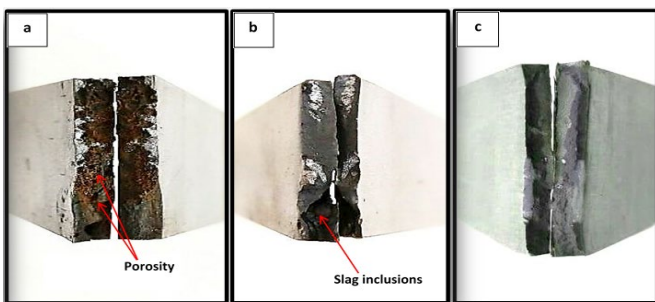


Figure 9. Fractography of the tensile test specimen of (a): oxy-acetylene weld, (b and c): SMA weld

4. CONCLUSIONS

The most important results of welding a 6 mm thick AISI 5160 steel plates using the SMAW and OAW processes can be deduced as follows:

- (1) The visual HAZ extension from the centerline of the oxy-acetylene weld (79.6 mm) was significantly greater than that of the SMA weld (23.6 mm).
- (2) The microstructures of both SMA and oxy-acetylene low alloy steel weld metals were generally ferrite and pearlite. The micrograph observation revealed that the pearlite structure in the grain growth region of the oxy-acetylene weld was much coarser than that of the SMA weld. The fusion zone of the oxy-acetylene weld was coarser as well.
- (3) The hardness values across the oxy-acetylene weld were generally lower than those found across the SMA weld.
- (4) The maximum hardness across both SMA and oxy-acetylene welds (380HV and 210HV respectively) was located in the CGHAZ region adjacent to the WZ, while the lowest (182HV and 125HV respectively) was found in the inter-critical HAZ region.
- (5) Across both welds, the center displayed lower average hardness compared to the BM. The hardness measured at the centre of the SMA weld (123HV) was however lower than that of the oxy-acetylene weld (149HV).
- (6) The average tensile strength and joint efficiency of the SMA weld (534MPa and 73.8%) were notably much higher than those of the oxy-acetylene weld (34.6MPa and 4.8%).
- (7) There were slag inclusions in one of the two fractured tensile test specimens of the SMA weld, whereas the other specimen showed a semi-ductile fracture in the weld. Fractography observation revealed the presence of pores and an oxide layer, and the fracture was brittle in the oxy-acetylene weld specimens.

5. RECOMMENDATIONS

There are several proposals for further investigations:

- (1) Carrying out impact testing on AISI 5160 steel welds to evaluate their fracture toughness.
- (2) Comparing welds achieved using other arc welding techniques, such as GMAW and SAW, with each other.
- (3) Investigating certain internal weld defects employing X-ray radiography.
- (4) Studying residual stress distribution through the welds.

REFERENCES

- [1] Phillips, D.H. (2023). *Welding Engineering: An Introduction*. John Wiley & Sons. 2nd ed., Wiley, United Kingdom.
- [2] Norrish, J. (2006). *Advanced Welding Processes. Technologies and Process Control*. Woodhead publishing limited, Cambridge, England.
- [3] Lancaster, J.F. (1999). *Metallurgy of Welding*. 6th ed., Woodhead Publishing Limited, Cambridge, England.
- [4] Bardes, B.P. (1978). *Metals Handbook, Vol. 1: Properties and Selection-Irons and Steels*. American Society For Metals.
- [5] Weman, K. (2012). *Welding Processes Handbook Second Edition*. Woodhead Publishing.
- [6] Bohnart, E. (2018). *Welding: Principles and Practices*.

- McGraw-Hill Education.
- [7] Brumbaugh, J.E., Miller, R. (2007). AudelTM welding pocket reference. Wiley Publishing, Inc., Canada.
- [8] Jenney, C.L., O'Brien, A. (2001). Welding Handbook: Welding Science and Technology. Woodhead Publishing Ltd.
- [9] Smith, F. (2014). Trade of Pipefitting Phase 2 module 2 thermal processes unit 2 introduction to oxy-acetylene Welding. SOLAS. <https://www.academia.edu/22075588>
- [10] American Welding Society. (1978). Welding Handbook: Vol. 2. Welding Processes-arc and Gas Welding and Cutting, Brazing and Soldering. American Welding Society.
- [11] Davies, A.C. (1989). The science and practice of welding: Welding science and technology. Cambridge University Press.
- [12] Olawale, O., Ibitoye, S., Oluwasegun, K.M., Shittu, M.D., Ofoezie, R.C. (2012). Correlation between process variables in shielded metal-arc welding (SMAW) process and post weld heat treatment (PWHT) on some mechanical properties of low carbon steel welds. *Journal of Minerals and Materials Characterization and Engineering*, 11(9): 891-895. <https://doi.org/10.4236/jmmce.2012.119084>
- [13] Sumardiyanto, D., Susilowati, S.E. (2019). Effect of welding parameters on mechanical properties of low carbon steel API 5L shielded metal arc welds. *American Journal of Materials Science*, 9(1): 15-21. <https://doi.org/10.5923/j.materials.20190901.03>
- [14] Sar, M.H., Barrak, O.S., Al-Adili, A.S., Hussein, S.K., Hussein, A.K. (2020). Study the effect of filler material on microstructure of welding the carbon steel in shielded metal arc welding. *Journal of Mechanical Engineering Research and Developments*, 43(3): 408-416.
- [15] Pathak, D., Singh, R.P., Gaur, S., Balu, V. (2021). Influence of input process parameters on weld bead width of shielded metal arc welded joints for AISI 1010 plates. *Materials Today: Proceedings*, 38: 24-28. <https://doi.org/10.1016/j.matpr.2020.05.516>
- [16] Bodude, M.A., Momohjimoh, I. (2015). Studies on effects of welding parameters on the mechanical properties of welded low-carbon steel. *Journal of Minerals and Materials Characterization and Engineering*, 3(3): 142-153. <http://dx.doi.org/10.4236/jmmce.2015.33017>
- [17] Fathi, M.S.A., Ismael, Q., Saleh, K.A. (2019). An effect of welding type on the mechanical properties of welding joints. *International Journal of Mechanical and Production Engineering Research and Development*, 9(4): 699-707.
- [18] AZO Material. AISI 5160 alloy steel (UNS G51600). <https://www.azom.com/article.aspx?ArticleID=6743>, accessed on Sep. 26, 2012.
- [19] Nunes et al. (1993). *Metals Handbook: Welding, Brazing, and Soldering*. ASM International. <https://docs.google.com/file/d/0B3Mrzn2Z7-tSRmVLdDlxT2V4cHM/view>
- [20] MATHESON Select RG45 Solid Wire (GTAW) OxyFuel Welding Rods Choose Box Weight & Wire Diameter. <https://store.mathesongas.com/mathesonselectrg45solidwiregtawoxyfuelweldingrodschooseboxweightwire>
- [21] ASTM (2020). *Metals Test Method and Analytical Procedures: Annual book of ASTM standards*, ASTM International, West Conshohocken.
- [22] Khan, M.I. (2007). *Welding Science and Technology*. New Age International (P) Ltd.
- [23] Khanna, O.P. (1980). *Welding Technology: A text Book for Engineering Students*. Dhanpat Rai & Sons, Delhi.
- [24] Jilabi, A.S.J. (2024). Comparative analysis of electrode type on microstructure and mechanical properties in AISI 5155 low alloy steel welds. *Annales de Chimie Science des Matériaux*, 48(2):187-195. <https://doi.org/10.18280/acsm.480205>
- [25] Odebiyi, O.S., Adedayo, S.M., Tunji, L.A., Onuorah, M.O. (2019). A review of weldability of carbon steel in arc-based welding processes. *Cogent Engineering*, 6(1): 1609180. <https://doi.org/10.1080/23311916.2019.1609180>
- [26] Gomes, M.D.G.M.D.F., Almeida, L.H., Gomes, L.C.F.C., May, I.L. (1997). Effects of microstructural parameters on the mechanical properties of eutectoid rail steels. *Materials Characterization*, 39(1): 1-14. [https://doi.org/10.1016/S1044-5803\(97\)00086-7](https://doi.org/10.1016/S1044-5803(97)00086-7)
- [27] Gray, T.G.F. (1982). *Rational Welding Design*. Butterworth-Heinemann.

NOMENCLATURE

El.	Elongation, %
Tm	Melting temperature
T.S.	Tensile strength, mpa
wt.	Weight percentage, %
Y.S.	Yield strength, mpa

Greek symbols

Ø	electrode diameter, mm
---	------------------------

Subscripts

AISI	American iron and steel institute
ASTM	American standards for testing of materials
AWS	American welding society
BM	Base metal
CGHAZ	Coarse grained heat affected zone
DCEP	Direct current electrode positive
FGHAZ	Fine grained heat affected zone
HAZ	Heat affected zone
GMAW	Gas metal arc welding
OAW	Oxy-acetylene welding
SAW	Submerged arc welding
SEM	Scanning electron microscopy
SMAW	Shielded metal arc welding
HV	Vickers hardness
WZ	Weld zone